Control Engineering Practice 45 (2015) 22–36

Contents lists available at ScienceDirect

Control Engineering Practice

journal homepage: www.elsevier.com/locate/conengprac

Maneuverability modeling and trajectory tracking for fish robot

Pichet Suebsaiprom, Chun-Liang Lin *

Bioinformatic Computing and Control Laboratory, Department of Electrical Engineering, National Chung Hsing University, Taichung, Taiwan 402, ROC

ARTICLE INFO

Article history:
Received 4 February 2015
Received in revised form
20 August 2015
Accepted 20 August 2015

Keywords:
Fish robot
Maneuverability
Trajectory control
Modeling
Carangiform locomotion

ABSTRACT

This study develops a 6-DOF mathematical model for a robotic fish that considers surge, sway, heave, roll, pitch, and yaw. The model considers the conditions of a fish swimming in ocean current perturbations similar to the ocean current perturbations of the slender-body autonomous underwater vehicles. For swimming and turning behaviors, a nonlinear, dynamic, carangiform locomotion model is derived by using a planar four-link model. A 2-DOF barycenter mechanism is proposed to provide body stabilization and to serve as an actuating device for active control design. A barycenter control scheme is developed to change the center of gravity of the robot fish body by moving balancing masses along two axes. The projected torque on x and y axes propel pitch and roll angles to the desired settings. A Stabilizing controller, fish-tail mechanism, rigid body dynamics, and kinematics are incorporated to enable the fish robot to move in three dimensional space. Simulation results have demonstrated maneuverability and control system performance of the developed controller which is proposed to conduct path tracking of the robot fish as it swims under current perturbations.

1. Introduction

Underwater robots have recently been used in several applications, such as ocean development, ocean investigations, military operations, and marine-environment protection. Various applications, such as military defense and marine protection, require high-performance autonomous underwater vehicles (AUVs), especially for propulsion and maneuverability.

To achieve efficient propulsion, researchers have investigated and implemented various underwater robots that mimic fishes. Because of natural selection and evolution, although not necessary to meet the global optimality, many fish species have developed the most efficient mechanism to thrive in the aquatic environment. Their remarkable abilities can inspire innovative designs to improve the performance of AUVs that operate in and interact with underwater environment. This can benefit AUVs considerably (Sfakiotakis, Lane, Bruce & Davies, 1999). The highly efficient swimming mechanism of some pelagic fishes can inspire a novel propulsion fin design serving as an option to the novel thruster fin design to replace turbine thruster currently in use. These ideas have inspired researchers to focus on the fish swimming mechanisms, especially the carangiform and thunniform locomotion of fishes such as tuna, salmon, and shark (Colgate & Lynch, 2004; Anderson & Chhabra, 2002).

Carangiform locomotion uses the caudal fin and the posterior body for swimming and orientating. Carangiform and thunniform locomotion are body and/or caudal fin (BCF) modes of swimming. Fish use this behavior to generate high-speed swimming, high thrust and acceleration, and small-turning angles with low power consumption (Donley and Dickson, 2000; Wen, Wang, Wu & Liang, 2013). BCF swimming also generates low propulsion noise and a less conspicuous underwater cavitation. These advantages could be crucial for military and stealth applications.

To exploit these swimming mechanism advantages, this study developed a carangiform 4-link planar robot based on previous research (Nakashima & Ohgishi, 2003; Yu & Wang, 2005; Kim, Lee, Vo & Trung, 2008; Vo, Kim, Cho, Dang & Lee, 2009; Vo, Kim & Lee, 2012; Niku, 2001). Lagrange's formulation was used to develop the mathematical model of 4-link carangiform locomotion. The quasi-steady condition in Lighthill (1960) included hydrodynamic force details to consider the lift and lateral forces on the fish tail and body in Suebsaiprom and Lin (2012) and Suebsaiprom, Lin, and Saimek (2012). The model developed in this study includes turning behavior that was achieved by bending two active joints of a fish tail. The various bending angles enable the robot fish to turn at different turning speeds and radii. The swimming and turning models exhibit a major advantage that the robot requires fewer control inputs than the robots in Yu, Liu, and Wang (2006) and Yu, Tan, Wang, and Chen (2004) do. Yu et al. (2006) and Yu et al. (2004) developed fish robots by adding four servo motors to the tail of the fish, and four active joints to controlled swimming and orientation.

* Corresponding author.
E-mail address: chunlin@dragon.nchu.edu.tw (C.-L. Lin).

http://dx.doi.org/10.1016/j.conengprac.2015.08.010
0967-0661/

For maneuvering or hovering, the existing systems cannot fulfill the requirements of practical demands, such as agile movement and stationary attitude, i.e. to let the fish robot change its direction rapidly and make it stay still. Stabilization in a fish robot requires ascending and descending swimming, self-stabilizing function, and stationary stabilizing function. The stationary stabilizing function is especially required to make the robot capable of acting as a motionless object underwater. Suebsaiprom, Saimek, and Chaisawadi (2004) proposed the concept of 2-DOF balancing for a fish robot. The authors constructed four balancing bladder tanks, which were set on a reference platform inside the robot body. This enabled 2-DOF maneuverability control of pitch (θ) and roll (ϕ) rotations, but the system responses were slow. Liu, Yu, and Wang (2006) and Morgansen, Triplett, and Klein (2007) proposed a pair of pectoral fins to control the heaving and pitching of a fish robot, but this method required fin speed or forward swimming to create lift force, which is proportional to the angle of attack of the foils. When the fish robot operates in a hovering mode, it should be able to stay still. In this operation mode, pitch and roll motions are difficult to realize. The 1-DOF barycenter mechanism is another technique that was applied to a fish robot in Zhou, Cao, Wang, and Tan (2006) and AUVs in Refsnes (2007) and Refsnes, Sorensen, and Pettersen (2008). The mechanism changes the center of gravity (CG) position, creating a pitching moment.

To improve pitch and roll stabilization and hovering, this study proposes a 2-DOF barycenter mechanism (Suebsaiprom & Lin, 2013) and combines it with fish robot rigid body dynamic and kinematic models to achieve three-dimensional (3-D) motion. Stabilizing behavior simulations were conducted to test the feasibility of the proposed system by focusing on stationary and swimming stabilization. The simulation of the merged system reveals the feasibility of posturing, maneuvering, and locating the fish robot in a 3-D reference frame.

This study makes the following contributions. A complete mathematical model describing fish robot motion and tail movement is developed for a 4-link planar robot with carangiform locomotion and the hydrodynamic forces acted on each link. The 2-DOF barycenter mechanism models are derived to improve stabilization of the fish body in terms of pitch and roll motions. The novel design of the 2-DOF barycenter mechanism ensures passive stability by introducing equilibrium reaction forces between a balancing buoyancy tank and two sliding masses. This mechanism also enables the motion of the fish robot in 3-D space. The pitch angle can be varied to control the descending or ascending swimming motion of the rigid body with the roll angle of the rigid body self-stabilized. Because of the rigid body of the fish robot, a fish swimming model similar to the common slender body AUV model is advantageous. This is demonstrated by the operating environments of fish robots that are similar to AUVs that have been proposed by several studies. Several control methodologies have been developed for AUVs (Silvestre, Cunha, Paulino & Pascoal 2009; Healey & Lienard, 1993; Busch, 2009; Bo, Lei, Ru & Bai, 2009; Cook, 2007), which demonstrate the possibilities of the developed robot fish, which can operate in real environments such as open sea currents. The proposed model of fish robot thus exhibits advantages for control design. Moreover, the completed model, including oceanic disturbance, mimics the robot working in the ocean environments which is useful for nonlinear and robust control design in the future works.

2. Model and equation of motion

2.1. Rigid body motion

The 6-DOF motion of the fish body was analyzed in a north-east-down (NED) frame in relation to three translations (surge, sway, and heave) and three rotations (roll, pitch, and yaw), as shown in Fig. 1.

The 3-D motion of the rigid body of the robot can be investigated by considering three basic mathematical models based on swimming, turning, and stabilizing behaviors.

2.2. Forward and turning swimming locomotion

The carangiform and thunniform are the undulatory BCF mode, as shown in Fig. 2. The propulsive wave traverses the fish body in a direction opposite to the overall movement and at a speed greater than the overall swimming speed. Typical carangiform swimmers have a narrow peduncle and a tall forked caudal fin. These are among the swiftest of swimmers. The fastest of the carangiform are often placed in another category, known as thunniform swimmers. These fishes, including tuna and some sharks, have very low-drag body shapes, narrow peduncles, and tall lunate caudal fins (Colgate & Lynch, 2004).

The carangiform and thunniform are quite similar in the swimming dynamic model with a few differences in the head movement as shown in Fig. 2. The head movement also depends on the fish shape and side drag of fish body. In this study, we focus on the torpedo shape fish robot that is easier to establish and set up the 2-DOF barycenter mechanism inside a robot body. This torpedo shape is more similar to mackerel than tuna that the carangiform locomotion have been designed.

Fish swimming with carangiform locomotion undulates the last third of the length of the body with a small movement of the head, but increasing amplitude from the head toward the tail (Pietsch, 2014). The characteristics of this locomotion type are fast swimming, high maneuverability, and a low drag force. Note that the swimming efficiency of the carangiform kinetics, in terms of the drag force reduction, has a higher *Re* compared with other kinetics; for example, a carangiform swimmer typically swims at high *Re* around 10^5 while an anguilliform swimmer swims at *Re* around 10^4 in nature (Borazjani, 2008). This study focused on developing a mathematical model for a robot fish that performs carangiform swimming. The structure consists of one body link, two active tail links, and one passive caudal fin link. The head of the robot fish is considered a part of the same structure as the body, and its structure is shown in Fig. 3.

The equivalent model of the fish robot consists of 4 planar links and 4 masses, as shown in Fig. 4, where $a_{0,1,2,3}$ are the distances

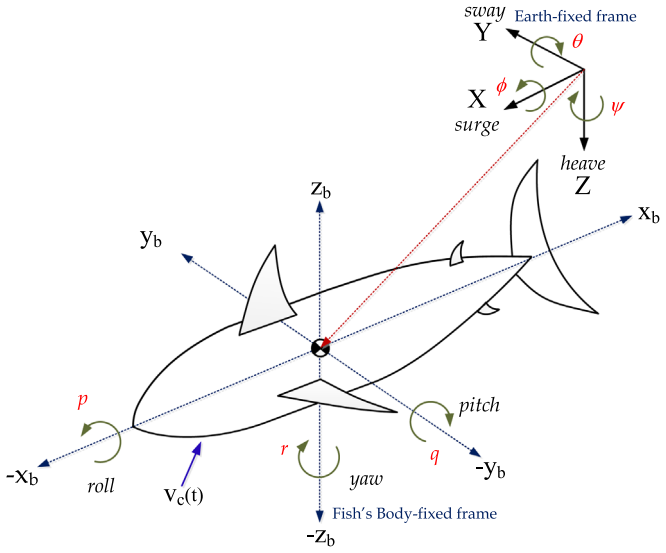

Fig. 1. Fish robot in the north-east-down (NED) frame.

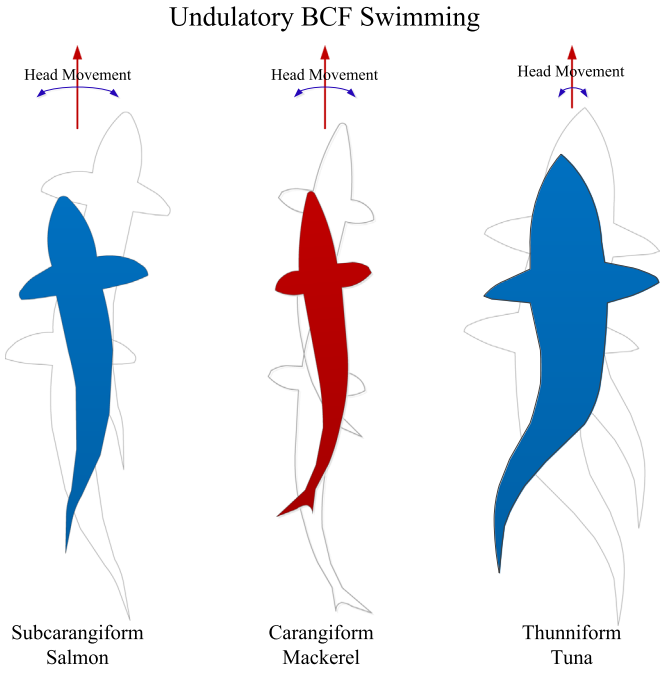

Fig. 2. Undulatory BCF swimming (Hoar & Randall, 1978).

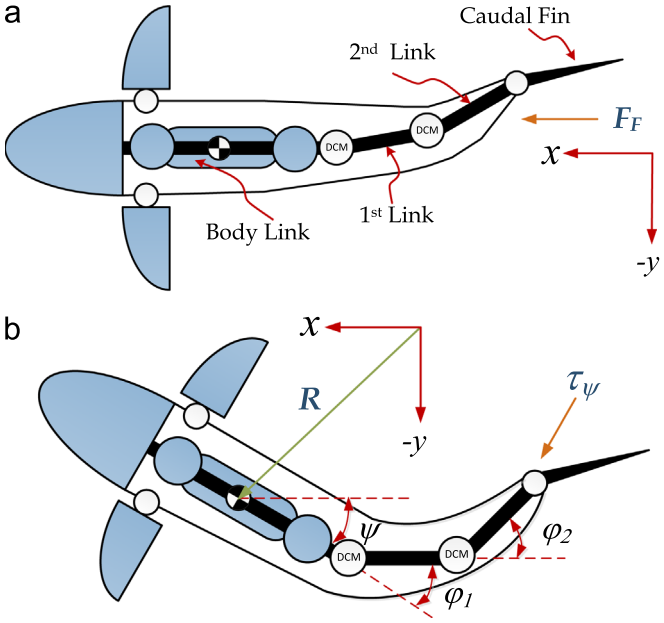

Fig. 3. Carangiform locomotion analyzed in 2-D space: (a) forward swimming and (b) multi-directional swimming.

from the joint to the center of mass of each link, $l_{0,1,2,3}$ are the lengths of each link, $\theta_{1,2,3}$ are the fish tail link angles, and θ_0 is the angle of the fish head swing during swimming. The optimization of link number and link–length-ratio has been investigated in Yu and Wang (2005). This 4-link ratio partly matches the construction of a biological fish. However, for practical concerns, the number of links cannot be unreasonably large, and the precise link–length-ratio is difficult to establish due to the limitations of the actuator size and the mechanical construction.

The dynamic fish tail model was developed by using Lagrange's equation. Considering different energy at the mass of each link, Lagrange's equation was applied to the equivalent model in Fig. 4 (a) and the forces acted on the fish tail are shown in Fig. 4(b). The head direction in $-x_b$ is set only in the fish's body-fixed frame for the convenient analysis of the fish tail motion. However, the rigid-body swimming direction is set at X direction (Fig. 1).

The dynamic fish robot model was obtained by using the following second order matrix form:

$$M(\boldsymbol{\theta}_i)\ddot{\boldsymbol{\theta}}_i + C(\boldsymbol{\theta}_i, \dot{\boldsymbol{\theta}}_i)\dot{\boldsymbol{\theta}}_i^2 + B\dot{\boldsymbol{\theta}}_i + K\boldsymbol{\theta}_i = \mathbf{F}_i \tag{1}$$

where $M(\boldsymbol{\theta}_i)$ is a moment of inertia matrix, $C(\boldsymbol{\theta}_i, \dot{\boldsymbol{\theta}}_i)$ is a Coriolis matrix, B is a damping coefficient matrix, K is a spring constant matrix, $\mathbf{F}_i$ is the force vector that includes hydrodynamic force, and $\boldsymbol{\theta}_i=[\theta_0\theta_1\theta_2\theta_3]^T$. Suebsaiprom and Lin (2012) and Suebsaiprom et al. (2012) have described the derivation in detail.

2.3. Hydrodynamic force on the fish tail

The hydrodynamic force represents the force acting on the fish robot tail. It can be defined as

$$F_V = \pi\rho LC^2\dot{U}\sin\alpha + \pi\rho LC^2\dot{\alpha}U\cos\alpha \tag{2}$$

$$F_J = 2\pi\rho LCU^2\sin\alpha\cos\alpha \tag{3}$$

where F_V is the force proportional to the acceleration acting in the opposite direction to the fish tail, F_J is the lift force acting in a perpendicular direction, C is the fin chord length, L is the fin tail span, ρ is the density of the water, α is the angle-of-attack at the tail fin, and U represents the flow relative speed at the center of the caudal fin. Because U_m and u_F are perpendicular, the value of U can be calculated by using

$$U^2 = U_m^2 + u_F^2 \tag{4}$$

where U_m is constant flow. If we consider only the movement of fish robot in forward direction, thus u_F is the relative velocity at the center of the fish tail in the y_b direction (Vo et al., 2012), which is determined by using

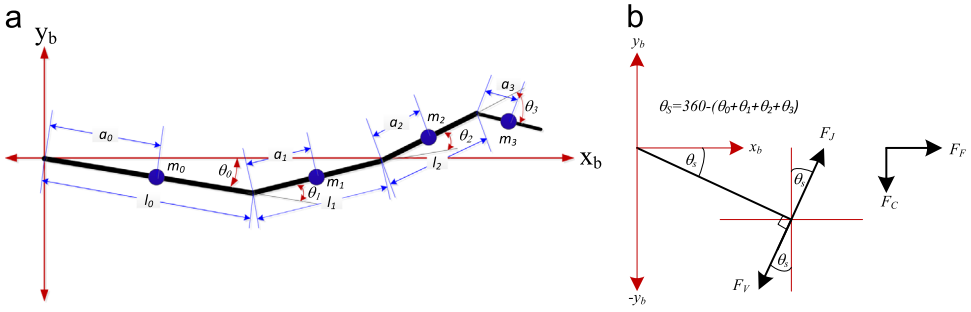

Fig. 4 (a). Equivalent model and (b) forces acting on fish tail.

$$u_F = l_0\dot{\theta}_0 \cos\theta_0 + l_1(\dot{\theta}_0 + \dot{\theta}_1)\cos(\theta_0 + \theta_1) + l_2(\dot{\theta}_0 + \dot{\theta}_1 + \dot{\theta}_2)\cos(\theta_0 + \theta_1 + \theta_2) + a_3(\dot{\theta}_0 + \dot{\theta}_1 + \dot{\theta}_2 + \dot{\theta}_3)\cos(\theta_0 + \theta_1 + \theta_2 + \theta_3) \quad (5)$$

For the behavior of sway force, the fish robot was pushed and pulled by this force that only caused little change of position in terms of the slide motion during swimming. Thus, the sway force is reasonably ignorable. Fluid force and lift force are divided into thrust component F_F on the x_b axis and lateral force component F_C on the y_b axis, respectively.

$$F_F = -F_V \sin(\theta_0 + \theta_1 + \theta_2 + \theta_3) + F_J \sin(\theta_0 + \theta_1 + \theta_2 + \theta_3) \quad (6)$$

$$F_C = F_V \cos(\theta_0 + \theta_1 + \theta_2 + \theta_3) - F_J \cos(\theta_0 + \theta_1 + \theta_2 + \theta_3) \quad (7)$$

The fish robot has two active joints, Joints 1 and 2, which generate the thrust force to the robot body. The two active joints are driven by two DC motors with identical input torque to simplify the analysis in control design that is described as

$$T_1 = A_T \sin(2\pi ft) \quad (8)$$

$$T_2 = A_T \sin(2\pi ft - \beta) \quad (9)$$

where A_T is the amplitude of input torque, f is the frequency of input torque, and β is the phase angle between the two input torques.

2.4. Balancing mechanism

Most fish have a center of buoyancy (CB) that is below their center of mass (CM), making their bodies naturally unstable. Most fish are also slightly negatively buoyant, despite having swim bladders that can be filled with gas or water. Therefore, when fish die or are anesthetized, they slowly turn upside down and sink (Lauder & Madden, 2006). To ensure that the fish robot body is naturally stable, a CB (artificial swim bladder), which is located above the CM, was designed, as depicted in Fig. 5. The fish robot is slightly positively buoyant, ensuring that it floats to the surface when it is in the event of robot failure, i.e. it stops moving for some reasons such as loss of electric power.

The 2-DOF barycenter mechanism changes the center of gravity inside the robot body by moving the balancing masses along the axes. The barycenter mechanism is set on a reference platform inside the fish robot, and the mechanism consists of two masses, two gear rails, two motors, and one buoyancy balancing tank. DC motors and gear boxes move the balancing masses along the x_b and y_b rails, respectively. Projections of the mass positions on the x_b and y_b axes create pitch and roll torques which are used to turn the robot fish to the desired angles. Fig. 5 shows the equivalent model.

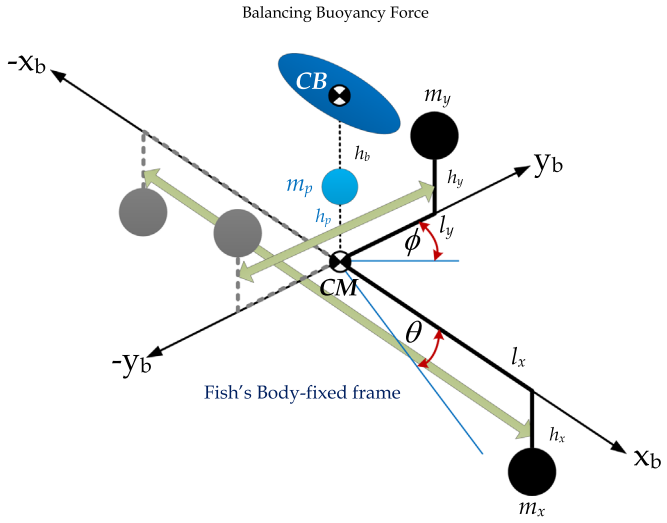

Fig. 5. Equivalent model of the balancing mechanism.

The buoyancy balancing tank was added to the system to ensure that the robot is naturally stable when the system is uncontrolled. In Fig. 5, m_x and m_y are movable masses along x_b and $y_b$axes, respectively; m_p is structure mass; B is buoyancy tank; l_x and l_y are distances from the movable masses to the center; h_x and h_y are the height of the masses along $z_b$axis; h_p is the height of m_p; and h_b is the length from CM to CB. The gray circles on $-x_b$ and $-y_b$ axes indicate the end position, which the mass m_x and m_y will move to. The lines with green arrows are parallel to x_b and y_b axes, which indicate the range where m_x and m_y will move along, respectively.

Similarly, the dynamic 2-DOF barycenter system model was developed based on Lagrange's equation, which considers the total energy of all the masses in the equivalent model by referring to the fixed frame of the fish body. The dynamic system model is written in the second order matrix form as follows:

$$\begin{bmatrix} I_{\theta 1} & I_{\theta 2} \\ I_{\phi 1} & I_{\phi 2} \end{bmatrix} \begin{bmatrix} \ddot{\theta} \\ \ddot{\phi} \end{bmatrix} = \begin{bmatrix} \tau_\theta \\ \tau_\phi \end{bmatrix} - \begin{bmatrix} \tau_{B\theta} \\ \tau_{B\phi} \end{bmatrix} - \begin{bmatrix} C_\theta \dot{\theta} \\ C_\phi \dot{\phi} \end{bmatrix} \quad (10)$$

where $I_{\theta i}$ and $I_{\phi i}$ are moment of inertia of the balancing system, τ_θ and τ_ϕ are input torques, $\tau_{B\theta}$ and $\tau_{B\phi}$ are balancing buoyancy forces acting in the opposite direction to the input torques, and C_θ and C_ϕ are damping coefficients. Terms in (10) are described as follows:

$$I_{\theta 1} = m_x l_x^2 + m_x h_x^2 + m_y h_y^2 + m_p h_p^2 + B h_b^2$$

$$I_{\theta 2} = m_y h_y l_y \sin(\theta)$$

$$I_{\phi 1} = m_y h_y l_y \sin(\theta)$$

$$I_{\phi 2} = m_y l_y^2 + \frac{1}{2}\{m_y h_y^2 + m_x l_x^2 + m_x h_x^2 + m_p h_p^2 + B h_b^2 + m_x h_x^2 \cos(2\theta) + m_y h_y^2 \cos(2\theta) + m_y l_y^2 \cos(2\theta) + m_p h_p^2 \cos(2\theta) + B h_b^2 \cos(2\theta)\} - m_x h_x l_x \sin(2\theta)$$

$$C_\theta = B_\theta + (m_p h_p^2 + B h_b^2)\sin^2(\theta)\sin(2\phi)$$

$$C_\phi = B_\phi + \frac{1}{2}\cos(\theta)\{4 m_x h_x l_x \cos(\phi) + 2[-2 m_x l_x^2 + 3 m_p h_p^2 + 3 B h_b^2 + (m_p h_p^2 + B h_b^2)\cos(2\phi)]\sin(\theta)\}$$

$$\tau_\theta = g\{-m_x l_x \cos(\theta)\cos(\phi) + m_y l_y \cos(\phi)\sin(\theta) + (-m_x h_x + m_p h_p)\cos(\phi)\sin(\theta)\}$$

$$\tau_\phi = g\{-m_y l_y \cos(\phi) + m_x l_x \cos(\theta)\sin(\phi) + (-m_x h_x + m_p l_p)\cos(\phi)\sin(\theta) + m_x l_x \sin(\phi)\sin(\theta)\}$$

$$\tau_{B\theta} = g B h_b \cos(\phi)\sin(\theta)$$

$$\tau_{B\phi} = g B h_b \cos(\theta)\sin(\phi)$$

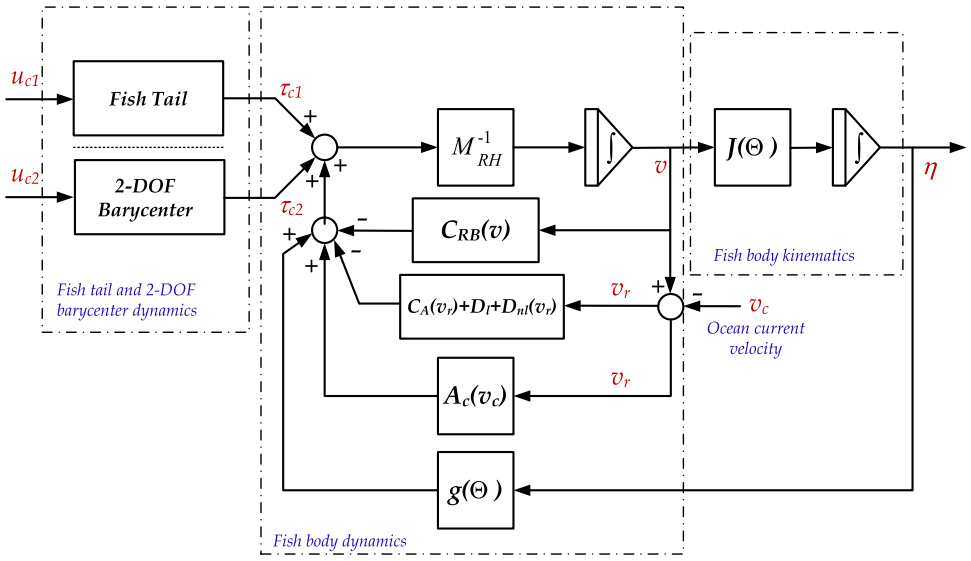

Fig. 6. Block diagram of the uncontrolled model.

2.5. Locomotion in a 3-D frame

The 6-DOF motion block diagram in the NED frame is shown in Fig. 6 that consists of fish-tail, stabilizing, and fish-body subsystems. The fish robot can be considered as a slender body underwater vehicle for which $\boldsymbol{\eta} = [x \;\; y \;\; z \;\; \phi \;\; \theta \;\; \psi]^T$ and $\mathbf{v} = [u \;\; v \;\; w \;\; p \;\; q \;\; r]^T$ are the generalized position and velocity vectors, respectively.

The kinetic relationship between the fixed frame of the fish body and the fish motion in the earth-fixed frame (Refsnes, 2007) is reflected in

$$\dot{\boldsymbol{\eta}} = J(\boldsymbol{\Theta})\mathbf{v} \tag{11}$$

where

$$J(\boldsymbol{\Theta}) = \begin{bmatrix} R(\boldsymbol{\Theta}) & 0 \\ 0 & T_\Theta(\boldsymbol{\Theta}) \end{bmatrix} \tag{12}$$

x and u are the surge position and velocity, respectively; y and v are the sway position and velocity, respectively; z and w are the heave position and velocity, respectively; ϕ and p are the roll angle and angular velocity, respectively; θ and q are the pitch angle and angular velocity, respectively; ψ and r are the yaw angle and angular velocity, respectively; $R(\boldsymbol{\Theta})$ is the linear velocity rotation matrix; $T_\Theta(\boldsymbol{\Theta})$ is the angular velocity transformation matrix; and $\boldsymbol{\Theta} = [\phi \;\; \theta \;\; \psi]^T$. $T_\Theta(\boldsymbol{\Theta})$ is singular at $\theta = \pm\pi/2$, meaning that the fish robot moves up or down perpendicular to the earth plane. The linear and angular velocity transformation matrices are defined as

$$R(\boldsymbol{\Theta}) = \begin{bmatrix} c(\psi)c(\theta) & -s(\psi)c(\phi) + c(\psi)s(\theta)s(\phi) & s(\psi)s(\phi) + c(\psi)c(\phi)s(\theta) \\ s(\psi)c(\theta) & c(\psi)c(\phi) + s(\phi)s(\theta)s(\psi) & -c(\psi)s(\phi) + s(\theta)s(\psi)c(\phi) \\ -s(\theta) & c(\theta)s(\phi) & c(\theta)c(\phi) \end{bmatrix} \tag{13}$$

$$T_\Theta(\boldsymbol{\Theta}) = \begin{bmatrix} 1 & s(\phi)t(\theta) & c(\phi)t(\theta) \\ 0 & c(\phi) & -s(\phi) \\ 0 & s(\phi)/c(\theta) & c(\phi)/c(\theta) \end{bmatrix} \tag{14}$$

where $c(.)=\cos(.)$, $s(.)=\sin(.)$, and $t(.)=\tan(.)$. Therefore, the equation of motion for the rigid body of the robot is

$$M_{RH}\dot{\mathbf{v}} + C_{RB}(\mathbf{v})\mathbf{v} = \boldsymbol{\tau}_\mathbf{H} \tag{15}$$

$$\boldsymbol{\tau}_\mathbf{H} = -C_A(\mathbf{v_r})\mathbf{v_r} - D(\mathbf{v_r})\mathbf{v_r} - g(\boldsymbol{\Theta}) + A_c(\mathbf{v_c})\mathbf{v_r} + \boldsymbol{\tau}_\mathbf{c} \tag{16}$$

where $\boldsymbol{\tau}_\mathbf{H}$ the is hydrodynamic force, $\mathbf{v_r}$ is the relative velocity between robot and current velocities, $\mathbf{v_c}$ is the ocean's current velocity, $\boldsymbol{\tau}_\mathbf{c}$ the is control force vector, $M_{RH} = M_{RB} + M_A$ is the mass matrix, and m_B is a fish robot mass and M_{RB} is the rigid-body mass matrix. Due to the hull's top-bottom and port-starboard geometric symmetry (Cooney, 2006), the hull added mass matrix M_A is defined as

$$M_{RB} = \begin{bmatrix} m_B & 0 & 0 & 0 & m_B z_G & 0 \\ 0 & m_B & 0 & -m_B z_G & 0 & m_B x_G \\ 0 & 0 & m_B & 0 & -m_B x_G & 0 \\ 0 & -m_B z_G & 0 & I_x & 0 & -I_{zx} \\ m_B z_G & 0 & -m_B x_G & 0 & I_y & 0 \\ 0 & m_B x_G & 0 & -I_{zx} & 0 & I_z \end{bmatrix} \tag{17}$$

$$M_A = \begin{bmatrix} M_{x\dot{u}} & 0 & 0 & 0 & 0 & 0 \\ 0 & M_{y\dot{v}} & 0 & 0 & 0 & M_{y\dot{r}} \\ 0 & 0 & M_{z\dot{w}} & 0 & M_{z\dot{q}} & 0 \\ 0 & 0 & 0 & M_{k\dot{p}} & 0 & 0 \\ 0 & 0 & M_{m\dot{w}} & 0 & M_{m\dot{q}} & 0 \\ 0 & M_{n\dot{v}} & 0 & 0 & 0 & M_{n\dot{r}} \end{bmatrix} \tag{18}$$

The rigid-body Coriolis matrix $C_{RB}(\mathbf{v})$ and the hydrodynamic Coriolis matrix $C_A(\mathbf{v})$ are shown in (19) and (20), respectively. The $C_A(\mathbf{v})$ matrix includes destabilizing Munk-moments. A Munk-moment arises because of the asymmetric location of the stagnation point, where the pressure is highest on the front of the body and lowest on the back.

$$C_{RB}(\mathbf{v}) = \begin{bmatrix} 0 & 0 & 0 & c_{41} & -c_{51} & -c_{61} \\ 0 & 0 & 0 & -c_{42} & c_{52} & -c_{62} \\ 0 & 0 & 0 & -c_{43} & -c_{53} & c_{63} \\ -c_{41} & c_{42} & c_{43} & 0 & -c_{54} & -c_{64} \\ c_{51} & -c_{52} & c_{53} & c_{54} & 0 & -c_{65} \\ c_{61} & c_{62} & -c_{63} & c_{64} & c_{65} & 0 \end{bmatrix} \tag{19}$$

where

$$c_{41} = m_B z_G r, \quad c_{42} = m_B w, \quad c_{43} = m_B (z_G p - \upsilon)$$

$$c_{51} = m_B (x_G q - w), \quad c_{52} = m_B (z_G r + x_G p), \quad c_{53} = m_B (z_G q + u),$$
$$c_{54} = I_{zx} p - I_{zr} r$$
$$c_{61} = m_B (x_G r + \upsilon), \quad c_{62} = -m_B u, \quad c_{63} = m_B x_G p, \quad c_{64} = I_y q,$$
$$c_{65} = I_{zx} r - I_x p$$

and

$$C_A(\mathbf{v}) = \begin{bmatrix} 0 & 0 & 0 & 0 & -c_{a3} & c_{a2} \\ 0 & 0 & 0 & c_{a3} & 0 & -c_{a1} \\ 0 & 0 & 0 & -c_{a2} & c_{a1} & 0 \\ 0 & -c_{a3} & c_{a2} & 0 & -c_{b3} & c_{b2} \\ c_{a3} & 0 & -c_{a1} & c_{b3} & 0 & -c_{b1} \\ -c_{a2} & c_{a1} & 0 & -c_{b2} & c_{b1} & 0 \end{bmatrix} \tag{20}$$

where

$$c_{a1} = M_{x\dot{u}} u, \quad c_{a2} = M_{y\dot{\upsilon}} \upsilon + M_{y\dot{r}} r, \quad c_{a3} = M_{z\dot{w}} w + M_{z\dot{q}} q$$

$$c_{b1} = M_{kp} p, \quad c_{b2} = M_{m\dot{w}} w + M_{m\dot{q}} q, \quad c_{b3} = M_{n\dot{\upsilon}} \upsilon + M_{n\dot{r}} r$$

The hydrodynamic damping is $D(\mathbf{v_r}) = D_l + D_{nl}(\mathbf{v_r})$, where D_l is the linear damping matrix and $D_{nl}(\mathbf{v_r})$ is the nonlinear damping (drag force) matrix. They are defined as

$$D_l = \begin{bmatrix} D_{xu} & 0 & 0 & 0 & 0 & 0 \\ 0 & D_{y\upsilon} & 0 & 0 & 0 & -D_{yr} \\ 0 & 0 & D_{zw} & 0 & D_{zq} & 0 \\ 0 & 0 & 0 & D_{kp} & 0 & 0 \\ 0 & 0 & D_{mw} & 0 & D_{mq} & 0 \\ 0 & -D_{n\upsilon} & 0 & 0 & 0 & D_{nr} \end{bmatrix} \tag{21}$$

$$D_{nl}(\mathbf{v_r}) = \begin{bmatrix} D_{|u|u}|u| & 0 & 0 & 0 & 0 & 0 \\ 0 & D_{|\upsilon|\upsilon}|\upsilon| & 0 & 0 & 0 & -D_{|\upsilon|r}|\upsilon| \\ 0 & 0 & D_{|w|w}|w| & 0 & D_{|w|q}|w| & 0 \\ 0 & 0 & 0 & D_{|p|p}|p| & 0 & 0 \\ 0 & 0 & D_{|q|w}|q| & 0 & D_{|q|q}|q| & 0 \\ 0 & -D_{|r|\upsilon}|r| & 0 & 0 & 0 & D_{|r|r}|r| \end{bmatrix} \tag{22}$$

In several marine applications, such as dynamic positioning and low speed operations, the equations of motion are derived based on the assumption that the angular velocities are low. However, adding a term to the equation of motion (16) improves this assumption. For the current change forces, rotation of the body-frame leads to a correspondingly changing body-fixed current velocity. This non-zero acceleration of the current velocity induces force on the object, which is described by the term $A_c(\mathbf{v_c})\mathbf{v_r}$ in (16). This $A_c(\mathbf{v_c})$ matrix yields

$$A_c(\mathbf{v_c}) = \begin{bmatrix} 0 & 0 & 0 & 0 & M_{x\dot{u}} w_c & -M_{x\dot{u}} v_c \\ 0 & 0 & 0 & -M_{y\dot{\upsilon}} w_c & 0 & M_{y\dot{\upsilon}} u_c \\ 0 & 0 & 0 & M_{z\dot{w}} v_c & -M_{z\dot{w}} u_c & 0 \\ 0 & 0 & 0 & 0 & 0 & 0 \\ 0 & 0 & 0 & M_{m\dot{w}} v_c & M_{m\dot{w}} u_c & 0 \\ 0 & 0 & 0 & -M_{n\dot{\upsilon}} w_c & 0 & M_{n\dot{\upsilon}} u_c \end{bmatrix} \tag{23}$$

The force vector includes the forces and moments generated by the fish tail and 2-DOF barycenter stabilization subsystem. This study mainly considers the following force vector:

$$\boldsymbol{\tau}_c = \begin{bmatrix} \boldsymbol{\tau}_{c1}^T & \boldsymbol{\tau}_{c2}^T \end{bmatrix}^T = \begin{bmatrix} F_T & 0 & 0 & | & \tau_\phi & \tau_\theta & \tau_\psi \end{bmatrix}^T \tag{24}$$

where F_T, τ_ϕ, τ_θ, and τ_ψ represent the generated surge force and roll, pitch, and yaw moments, respectively. Because the small effect of sway force is negligible, the thrust force and turn moment are defined, respectively, as

$$F_T = \cos(\varphi_T) F_F \tag{25}$$

$$\tau_\psi = l_\tau \sin(\varphi_T) F_F \tag{26}$$

where $\varphi_T = \varphi_1 + \varphi_2$ is the total folding angle of the fish tail where φ_1 and φ_2 are the blending angles of Link 1 and Link 2, respectively; l_τ is the length from the rigid-body pivot to the point where the control force is applied, which can be approximated by $l_\tau = l_0 + l_1 \cos(\varphi_1) + l_2 \cos(\varphi_T)$.

In the buoyancy force vector, $g(\boldsymbol{\Theta})$, the weight of the submerged body is defined as $W = m_B g$, where g is gravity and the buoyancy force is defined as $B = \rho g \nabla$, where ∇ represents the submerged volume. A slightly buoyant vehicle was considered (i.e., $B = \delta + W$), where δ is a small positive number that adds a small positive buoyancy value to ensure that the fish body floats on the sea surface if it is failure during operation in deep water. Thus, the buoyancy force vector is

$$g(\boldsymbol{\Theta}) = \begin{bmatrix} (B - W) s(\theta) \\ (W - B) c(\theta) s(\phi) \\ (W - B) c(\theta) c(\phi) \\ (z_B B - z_G W) c(\theta) s(\phi) + (y_B B - y_G W) c(\theta) c(\phi) \\ (z_B B - z_G W) s(\phi) + (x_B B - x_G W) c(\theta) c(\phi) \\ (x_B B - x_G W) c(\theta) s(\phi) + (y_B B - y_G W) s(\phi) \end{bmatrix} \tag{27}$$

$\mathbf{r_G} = [x_G \;\; y_G \;\; z_G]$ is the position vector from the body origin to the center of gravity. For underwater vehicles, if x_G, x_B, and z_G equal zero at the origin and y_G and y_B equal zero at the port-starboard symmetry point, then the buoyancy force vector can be rewritten as

$$g(\boldsymbol{\Theta}) = \begin{bmatrix} (B - W) s(\theta) \\ (W - B) c(\theta) s(\phi) \\ (W - B) c(\theta) c(\phi) \\ z_B B c(\theta) s(\phi) \\ z_B B s(\phi) \\ 0 \end{bmatrix} \tag{28}$$

where (x_B, y_B, z_B) denotes the position from the body origin to the CB.

2.6. Ocean current modeling

Ocean currents considerably affect the motion and stability of a fish robot. The currents generate a relative velocity between the water flow and the robot's body, and have a hydrodynamic effect on the fish robot. The current velocity can be modeled as a Gauss–Markov process (Refsnes et al., 2008) as follows:

$$\dot{V}_c(t) + \mu_c V_c(t) = w_c(t) \tag{29}$$

where $w_c(t)$ is Gaussian white noise, and $\mu_c > 0$ is a suitable constant, and the limitation of current speed is defined by

$$V_{min} \le V_c(t) \le V_{max} \tag{30}$$

Assume that the fluid is irrotational; the current velocity vector in the NED-frame is given by

$$\mathbf{v}_c^e = \begin{bmatrix} \upsilon_x & \upsilon_y & \upsilon_z & 0 & 0 & 0 \end{bmatrix}^T \tag{31}$$

where $\upsilon_x = V_c \cos(\varphi_c) \cos(\phi_c)$

$\upsilon_y = V_c \sin(\varphi_c) \cos(\phi_c)$

$$v_z = V_c \sin(\phi_c)$$

$$V_c = \sqrt{v_x^2 + v_y^2 + v_z^2}$$

The current vector components are represented in north, east and down directions, and φ_c and ϕ_c are horizontal and vertical current angles, respectively. In underwater environments with substantial variety in depth and bottom topology, a vertical current component must be included. In general, the horizontal angle (φ_c) and vertical angle (ϕ_c) randomly change. Moreover, the NED-frame current velocity can be transformed into the body frame as

$$\mathbf{v_c} = diag\left[R^T(\Theta), 0_{3\times3}\right]\mathbf{v}_c^e$$

$$= \left[u_c \;\; v_c \;\; w_c \;\; 0 \;\; 0 \;\; 0\right]^T \tag{32}$$

where u_c, v_c, and w_c denote the current speed reacting in surge, sway, and heave, respectively. As a result, the relative velocity is defined as follows

$$\mathbf{v_r} = \mathbf{v} - \mathbf{v_c} = \left[u_r \;\; v_r \;\; w_r \;\; p \;\; q \;\; r\right]^T \tag{33}$$

3. Maneuverability and trajectory control

3.1. Maneuverability control

Control of the fish robot considered here can be divided into three parts: speed control referring to swimming velocity tracking control, orientation control referring to yaw tracking control, and stabilization control referring to pitch and roll tracking control. Three linearized models of each behavior were developed under the assumption that the fish velocity only changes slightly by means of the equilibrium point of vector v, which are set to be zero. Thus, three simplified linearized models (Healey & Lienard, 1993) of the decoupled fish dynamics were used for control design.

3.2. Speed control

The linearized model of fish speed can be written in a simplified form by using small perturbation theory (Bo et al., 2009) and neglecting the effect of small pitch rate perturbation, resulting in the following linearized equation:

$$\dot{u} = a_u u + b_u A_T \tag{34}$$

$$y_u = c_u u \tag{35}$$

where $a_u = -D_{xu}/(m_B + M_{x\dot{u}})$, $b_u = \alpha_T/(m_B + M_{x\dot{u}})$, $c_u = 1$, α_T is proportional thrust force gain, and A_T is defined in (8) and (9). The system with the type 1 servo controller (Ogata, 1994) is considered to be

$$\begin{bmatrix}\dot{u}\\ \dot{\xi}_u\end{bmatrix} = \begin{bmatrix}a_u & 0\\ -c_u & 0\end{bmatrix}\begin{bmatrix}u\\ \xi_u\end{bmatrix} + \begin{bmatrix}b_u\\ 0\end{bmatrix}u_u + \begin{bmatrix}0\\ 1\end{bmatrix}u_r \tag{36}$$

$$\widehat{y_u} = \begin{bmatrix}c_u & 0\end{bmatrix}\begin{bmatrix}u\\ \xi_u\end{bmatrix} \tag{37}$$

where u is the swimming velocity and $\dot{\xi}_u = u_r - u(t)$. The continuous-time linear quadratic regulator (LQR) problem was solved to minimize the performance index

$$J_u = \int_0^\infty \left(\mathbf{e}_u^T Q_u \mathbf{e}_u + u_u^2 r_u\right)dt \tag{38}$$

The associated reduced-matrix Riccati equation is

$$\widehat{A}_u^T P_u + P_u \widehat{A}_u - \frac{1}{r_u} P_u \widehat{B}_u \widehat{B}_u^T P_u + Q_u = 0 \tag{39}$$

where $P_u = P_u^T = [p_{u,ij}]_{2\times2}$, $\widehat{A}_u = \begin{bmatrix}a_u & 0\\ -c_u & 0\end{bmatrix}$, $\widehat{B}_u = \begin{bmatrix}b_u\\ 0\end{bmatrix}$, $Q_u = Q_u^T \geq 0$, $\mathbf{e}_u$ is $[u \;\; \xi_u]^T$, $u_u = A_T$, and $r_u > 0$.

The optimal speed control law is

$$u_{ue} = -K_u u + K_u^I \xi_u \tag{40}$$

where P_u is the unique solution to (39), K_u is the state feedback gain, and K_u^I is the error integral gain of the velocity control loop.

3.3. Orientation control

The linearized fish orientation model is written in the simplified state-space form as

$$\dot{\mathbf{d}} = A_r \mathbf{d} + B_r \varphi_T \tag{41}$$

$$y_r = C_r \mathbf{d} \tag{42}$$

where

$$A_r = \begin{bmatrix}1 & 0 & 0\\ 0 & I_z + M_{n\dot{r}} & M_{n\dot{v}}\\ 0 & M_{y\dot{r}} & m_B + M_{y\dot{v}}\end{bmatrix}^{-1}\begin{bmatrix}0 & 1 & 0\\ 0 & -D_{nr} & D_{nv}\\ 0 & D_{yr} & -D_{yv}\end{bmatrix}$$

$$B_r = \begin{bmatrix}1 & 0 & 0\\ 0 & I_z + M_{n\dot{r}} & M_{n\dot{v}}\\ 0 & M_{y\dot{r}} & m_B + M_{y\dot{v}}\end{bmatrix}^{-1}\begin{bmatrix}0\\ b_r\\ b_v\end{bmatrix}, \quad C_r = \begin{bmatrix}c_r & 0 & 0\end{bmatrix},$$

$$\mathbf{d} = \begin{bmatrix}\psi & r & v\end{bmatrix}^T$$

and $\dot{\xi}_r = \psi_r - \psi(t)$, $c_r = 1$, b_r and b_v are proportional turning and swaying gains, respectively; ψ is yaw angle, and r is yaw angular velocity. The same method used to achieve orientation control was applied to type 1 servo control design. The system equation with control input is rewritten as

$$\begin{bmatrix}\dot{\mathbf{d}}\\ \dot{\xi}_r\end{bmatrix} = \begin{bmatrix}A_r & 0\\ -C_r & 0\end{bmatrix}\begin{bmatrix}\mathbf{d}\\ \xi_r\end{bmatrix} + \begin{bmatrix}B_r\\ 0\end{bmatrix}u_T + \begin{bmatrix}0\\ 1\end{bmatrix}\psi_r \tag{43}$$

$$\widehat{y_r} = \begin{bmatrix}C_r & 0\end{bmatrix}\begin{bmatrix}\mathbf{d}\\ \xi_r\end{bmatrix} \tag{44}$$

To control the orientation, the continuous-time LQR problem was solved for yaw control to minimize the performance index and the control law.

3.4. Stabilizing control for pitch and roll

The linearized model of the stabilization system is shown in the decoupling form as follows:

$$\dot{\mathbf{s}} = A_s \mathbf{s} + B_s \mathbf{u_s} \tag{45}$$

$$\mathbf{y_s} = C_s \mathbf{s} \tag{46}$$

where

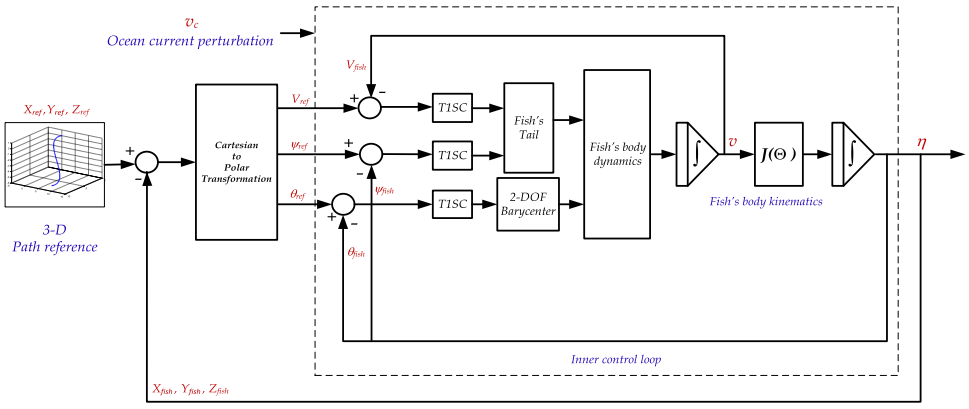

Fig. 7. Inner and outer loop control diagram for the fish robot.

Table 1
Fish robot parameters.

$m_B = 4.0$ kg	$l_B = 1.0$ m	$\varnothing_B = 0.25$ m
$I_x = 0.1422$ kg m^2	$I_y = 0.2836$ kg m^2	$I_z = 0.1789$ kg m^2
$I_{zx} = 0.0360$ kg m^2	$x_G = y_G = z_G = 0$ m	$x_B = y_B = 0$ m
$W = 39.2$ N	$B = 39.6$ N	$z_B = h_B = 0.05$ m

Note: l_B is the length of the fish body and $\varnothing_B$ is the diameter.

$$A_s = \begin{bmatrix} 0 & 1 & 0 & 0 \\ a_{21} & a_{22} & 0 & 0 \\ 0 & 0 & 0 & 1 \\ 0 & 0 & a_{43} & a_{44} \end{bmatrix}, \quad B_s = \begin{bmatrix} 0 & 0 \\ b_1 & 0 \\ 0 & 0 \\ 0 & b_2 \end{bmatrix}, \quad C_s = \begin{bmatrix} 1 & 0 & 0 & 0 \\ 0 & 0 & 1 & 0 \end{bmatrix}$$

with

$$a_{21} = \frac{-g[-m_x h_x + m_y h_y - m_p h_p + B h_b]}{I_{\phi 0} + I_x + M_{k\dot{p}}}, \quad a_{22} = \frac{-(C_\phi + D_{kp})}{I_{\phi 0} + I_x + M_{k\dot{p}}}$$

$$a_{43} = \frac{-g[-m_x h_x + m_y h_y - m_p h_p + B h_b]}{I_{\theta 0} + I_y + M_{m\dot{q}}}, \quad a_{44} = \frac{-(C_\theta + D_{mq})}{I_{\theta 0} + I_y + M_{m\dot{q}}}$$

$$b_1 = \frac{-g m_x}{I_{\phi 0} + I_x + M_{k\dot{p}}}, \quad b_2 = \frac{-g m_y}{I_{\theta 0} + I_y + M_{m\dot{q}}}$$

and

$$I_{\phi 0} = I_{\theta 0} = m_x h_x^2 + m_y h_y^2 + m_p h_p^2 + B h_b^2$$

The type 1 servo control was applied to the stabilization loop. The control design model was rewritten as

$$\begin{bmatrix} \dot{\mathbf{s}} \\ \dot{\boldsymbol{\xi}}_{\mathbf{s}} \end{bmatrix} = \begin{bmatrix} A_s & 0 \\ -C_s & 0 \end{bmatrix} \begin{bmatrix} \mathbf{s} \\ \boldsymbol{\xi}_{\mathbf{s}} \end{bmatrix} + \begin{bmatrix} B_s \\ 0 \end{bmatrix} \mathbf{u_s} + \begin{bmatrix} 0 \\ I \end{bmatrix} \mathbf{S_r} \tag{47}$$

$$\widehat{\mathbf{y}}_{\mathbf{s}} = \begin{bmatrix} C_s & 0 \end{bmatrix} \begin{bmatrix} \mathbf{s} \\ \boldsymbol{\xi}_{\mathbf{s}} \end{bmatrix} \tag{48}$$

where $\mathbf{s} = [\phi \ \dot{\phi} \ \theta \ \dot{\theta}]^T$, $\boldsymbol{\xi}_{\mathbf{s}} = [\xi_\phi \ \xi_\theta]^T$, $\mathbf{u_s} = [l_y \ l_x]^T$, $\mathbf{S_r} = [\phi_r \ \theta_r]^T$, $\dot{\xi}_\phi = \phi_r - \phi(t)$, and $\dot{\xi}_\theta = \theta_r - \theta(t)$. The LQR control design was also applied and the performance index was solved for the control gain design.

3.5. Guidance and trajectory control

The line-of-sight (LOS) guidance for the fish robot includes a heading subsystem and a pitching guidance subsystem. Fish heading guidance is derived from the location error related to the X and Y axes as follows:

Table 2
Hydrodynamic parameters of the fish robot.

Added mass	Linear damping coefficients	Nonlinear damping coefficients
$M_{x\dot{u}} = 0.62$ kg	$D_{xu} = 4.0$	$D_{|u|u} = 0.76$
$M_{y\dot{v}} = 4.60$ kg	$D_{yv} = 6.0$	$D_{|v|v} = 28.69$
$M_{z\dot{w}} = 4.60$ kg	$D_{zw} = 5.0$	$D_{|w|w} = 28.69$
$M_{k\dot{p}} = 0.04$ kg m^2	$D_{kp} = 2.0$	$D_{|p|p} = 1.32$
$M_{m\dot{q}} = 0.20$ kg m^2	$D_{mq} = 2.0$	$D_{|q|q} = 1.38$
$M_{n\dot{r}} = 0.20$ kg m^2	$D_{nr} = 6.0$	$D_{|r|r} = 1.38$
$M_{z\dot{q}} = M_{m\dot{w}} = 2.30$ kg m	$D_{zq} = D_{mw} = 1.5$	$D_{|w|q} = D_{|q|w} = 1.2$
$M_{y\dot{r}} = M_{n\dot{v}} = 2.30$ kg m	$D_{yr} = D_{nv} = 1.5$	$D_{|v|r} = D_{|r|v} = 1.2$

$$r_{2D} = \sqrt{e_x^2 + e_y^2} \tag{49}$$

$$\psi_{ref} = \tan^{-1}\left(\frac{e_y}{e_x}\right) \tag{50}$$

where r_{2D} is the error of length and ψ_{ref} is the reference command for the orientation control loop. Heading angle ψ_{ref} is obtained trigonometrically from the straight line between the current and waypoint. The fish robot heading is calculated by using (50), which follows the conventional sign. Positive angles ($0^\circ < \psi_{ref} \le 180^\circ$) refer to the starboard side and negative angles ($-180^\circ < \psi_{ref} < 0^\circ$) refer to the port side (McGookin, Murray-Smith, Li, & Fossen, 2000). Similarly, the pitching guidance is calculated by using

$$\theta_{ref} = -\tan^{-1}\left(\frac{e_z}{r_{2D}}\right) \tag{51}$$

$$V_{ref} = \alpha_v \sqrt{e_x^2 + e_y^2 + e_z^2} \tag{52}$$

where V_{ref} is the reference command in the speed control loop; θ_{ref} is the reference command for the pitch control loop; $e_x = X_{wp}(t) - X(t)$; $e_y = Y_{wp}(t) - Y(t)$; $e_z = Z_{wp}(t) - Z(t)$ is the position error between the current position and reference waypoint; $(X_{wp}(t), Y_{wp}(t), Z_{wp}(t))$ is the reference waypoint position; $(X(t), Y(t), Z(t))$ is the fish robot position; and α_v is the proportional control gain for the trajectory tracking loop. $\theta_{ref} > 0$ refers to the descending swimming and $\theta_{ref} < 0$ refer to the ascending swimming. Thus, the reference input is defined as $(u_r, \psi_r, \theta_r) = (V_{ref}, \psi_{ref}, \theta_{ref})$. For self-stabilization of the roll angle, ϕ_r is to zero. Fig. 7 shows

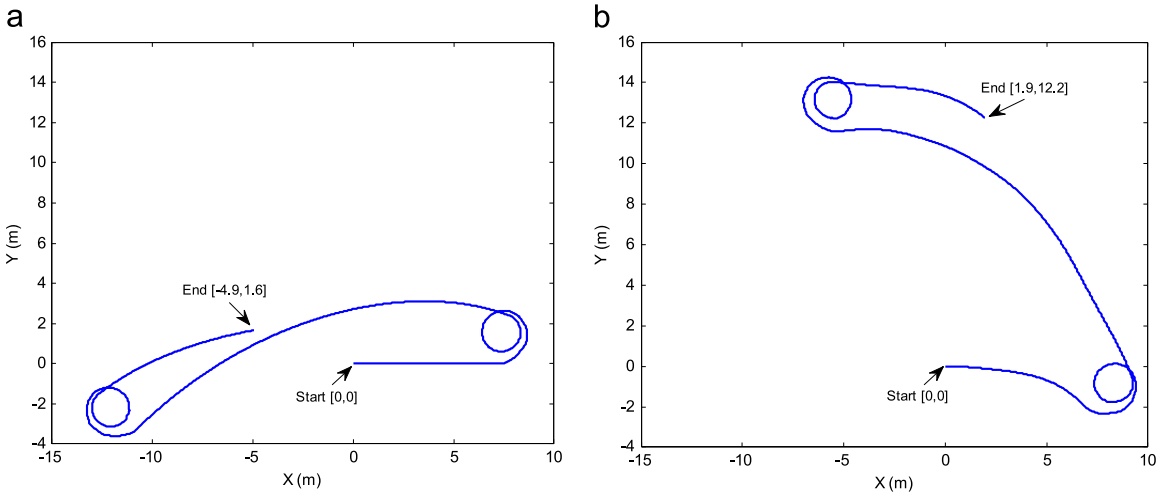

Fig. 8. Uncontrolled swimming and turning: (a) without ocean current perturbations and (b) with ocean current perturbations $|V_c|=0.5$ m/s.

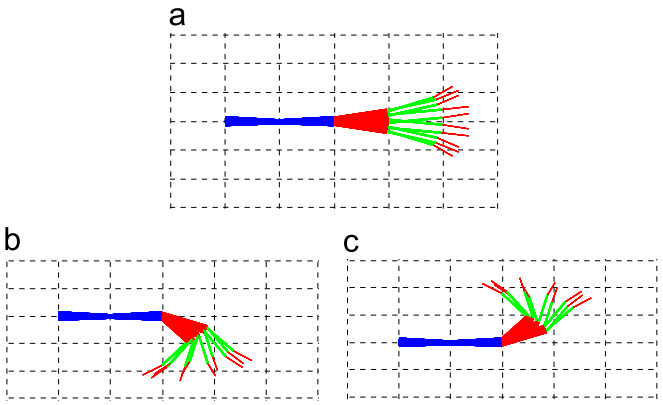

Fig. 9. Link locomotion of the robot body during forward and multi-directional swimming: (a) forward swimming, (b) CCW turn by blending the first and second tail links at $\varphi_T=-90°$, and (c) CW turn by blending the first and second tail links at $\varphi_T=90°$.

block diagram of the guidance and control systems.

4. Model verification and control design

To demonstrate the 6-DOF motion responses, physical parameters of the rigid body system were classified into two subsystems. Table 1 shows the parameters of the body of the fish robot. Table 2 shows the hydrodynamic parameters, such as added mass, coriolis, and drag coefficients.

For details of the fish tail and 2-DOF barycenter parameters one is referred to Suebsaiprom and Lin (2012, 2013). The physical size we considered is for a real-world fish robot which is currently under construction. The hydrodynamic parameters in Table 2 were estimated by using the formulas in Chan and Kang (2011); Techet (2005); Perrault, Bose, Young, and Williams (2003); Saout and

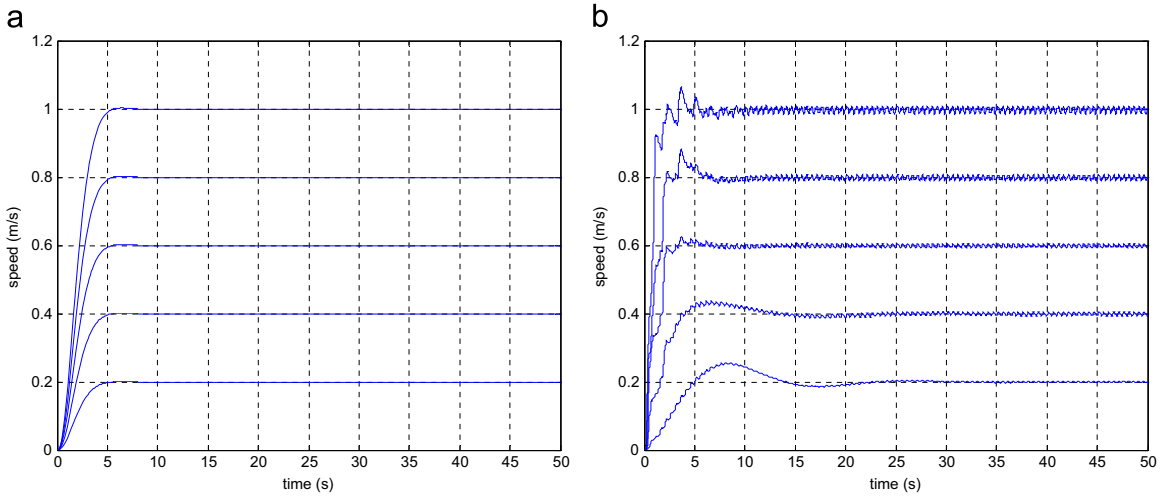

Fig. 10. Speed control of the fish robot under ocean currents: (a) linear model responses and (b) nonlinear model responses.

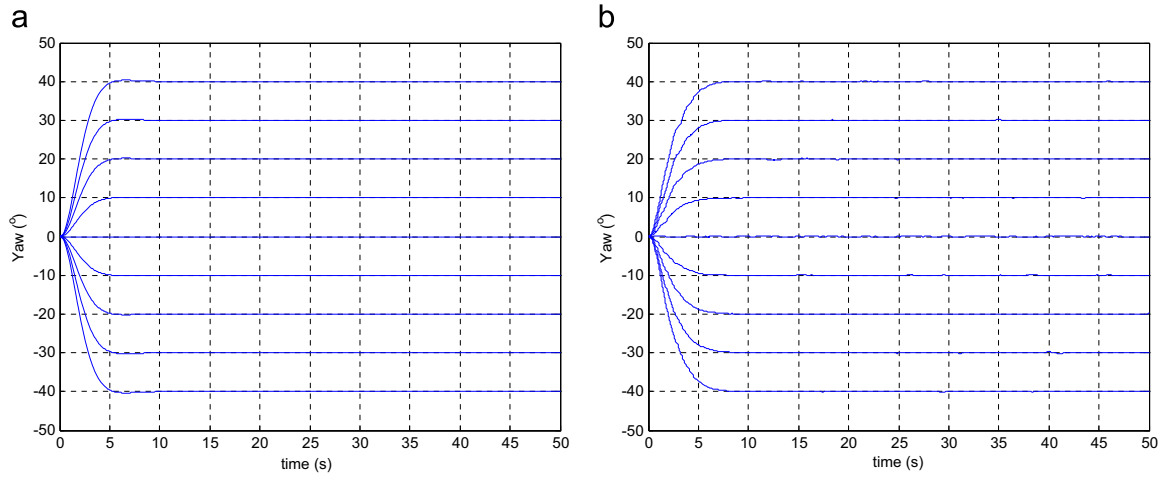

Fig. 11. Yaw angle tracking control in an ocean currents: (a) linear model responses and (b) nonlinear model responses.

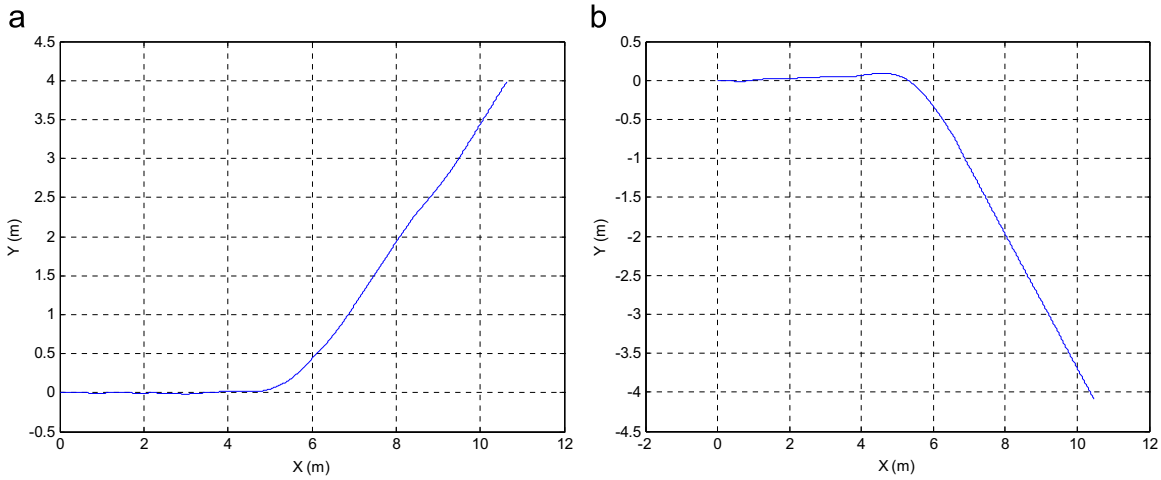

Fig. 12. Orientation control of the fish robot: (a) 40° turn and (b) −40° turn.

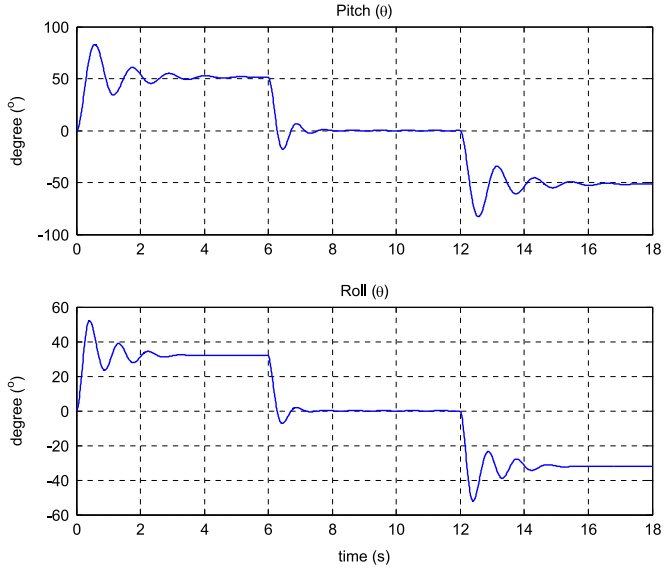

Fig. 13. Uncontrolled pitch and roll responses of the 2-DOF barycenter mechanism.

Ananthakrishnan (2011). The added mass, drag force, and linear damping should be considered from hull shape, body geometric, and application areas. A high-efficiency computer aided design and fluid analysis tool, such as Computational Fluid Dynamics (CFD), are necessary for analyzing the accurate hydrodynamic parameters.

To validate the feasibility of the proposed machine and control method, the simulation study examined two main factors. First, the fish robot maneuverability and the inner-loop control scheme based on the robot body frame are described. Second, 3-D path tracking behaviors in an NED frame are demonstrated.

4.1. *Maneuverability and inner-loop control*

Open-loop control of the swimming behavior of the rigid body were realized by using non-feedback oscillatory torques and bent angles to drive the motors, and the results show the path of the robot fish in a two-dimensional (2-D) reference frame in relation to *X* and *Y* axes. Fig. 8(a) shows that, without perturbations, the fish robot swam freely forward and turned. The effect of ocean current perturbations on the swimming path is shown in Fig. 8(b). In these conditions, the uncontrolled robot began to swim forward from 0 s to 10 s.

Fig. 9(a) shows animation of the body and tail link behaviors during swimming and turning. A deflecting angle ($\varphi_T = -90°$) has been added to the tail link to turn the fish robot in the counter-clockwise (CCW) direction. It swims forward again after 30 s. Fig. 9 (b) shows the turning behavior.

Fig. 9(c) shows the clockwise (CW) turning behavior. A

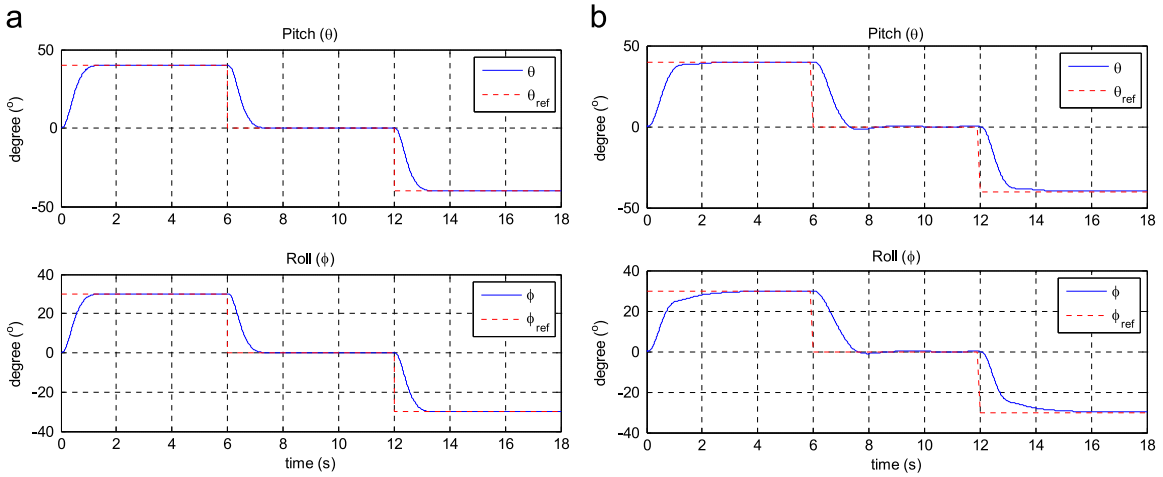

Fig. 14. Controlled pitch and roll responses of the 2-DOF barycenter mechanism: (a) linear model responses and (b) nonlinear model responses.

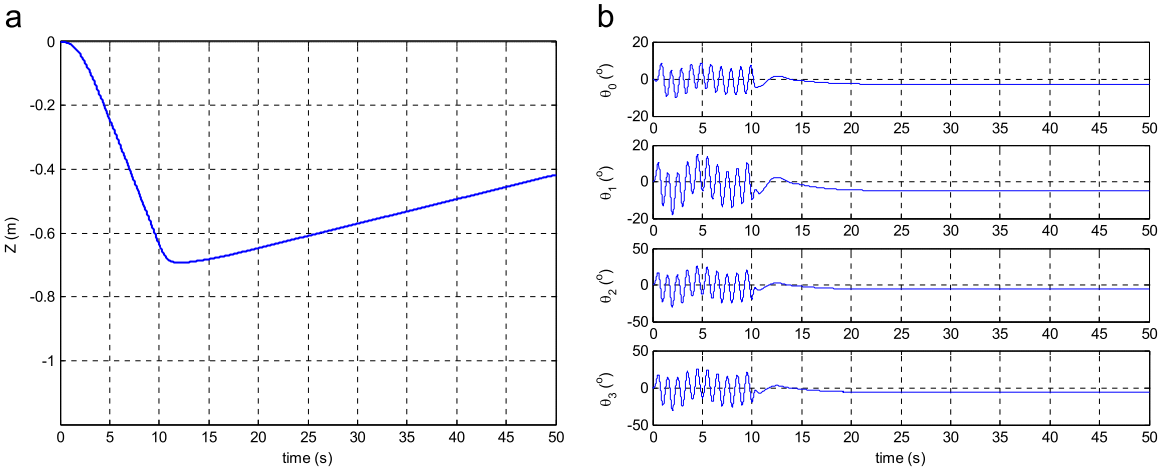

Fig. 15. Fish stopped operation under water: (a) heave slightly floating and (b) tail links behavior during stops to operate.

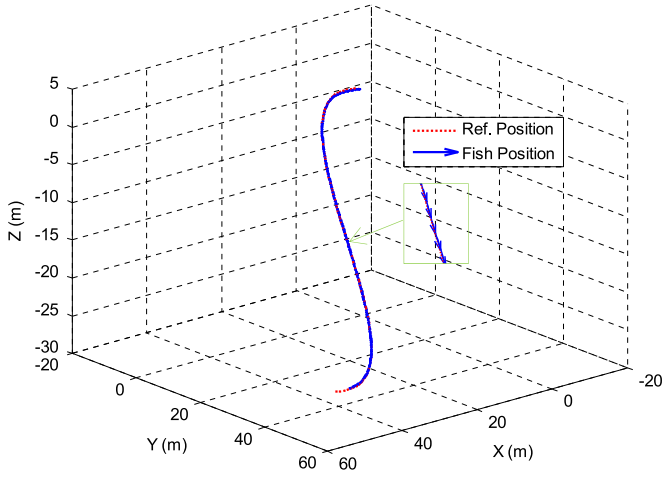

Fig. 16. 3-D trajectory tracking without ocean current perturbations.

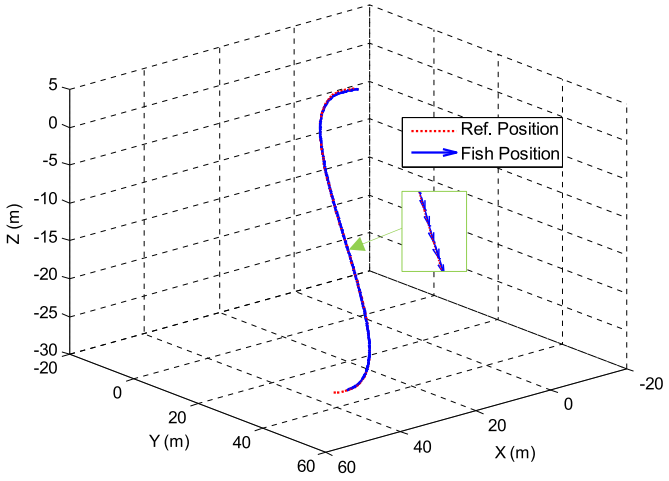

Fig. 17. 3-D trajectory tracking with ocean current perturbations of $|V_C|=0.5$ m/s.

deflecting angle ($\varphi_T=90°$) has been added to the tail link from 50 s to 70 s and the fish swims forward again after 70 s. However, water flow from the open ocean may significantly disturb the swimming locomotion, as shown in Fig. 8(a) and (b). Therefore, a navigation and control system is required to regulate the swimming position of the fish robot and reduce tracking errors.

Note that if we consider fin positions related to x_b, the position change related to x_b would be relatively small but large change related to y_b. For the situation of a bending tail, fin velocities in both directions can be transformed by using the rotational transformation at the total folding angle (φ_T). In this research, the velocity relative to x_b has been ignored for the sake of simpleness.

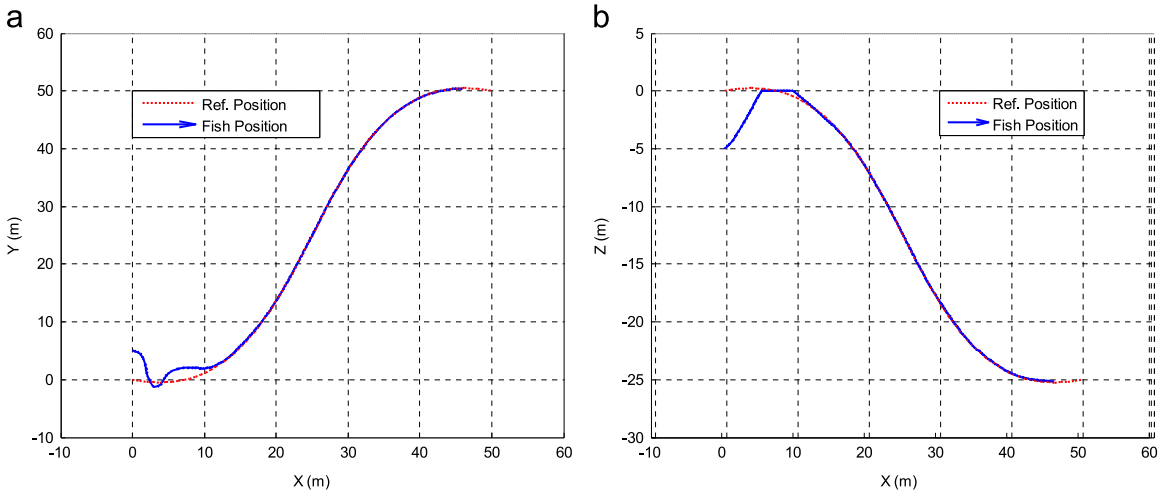

Fig. 18. Trajectory tracking with the initial condition: (a) 5 m on the *Y* axis and (b) −5 m on the *Z* axis.

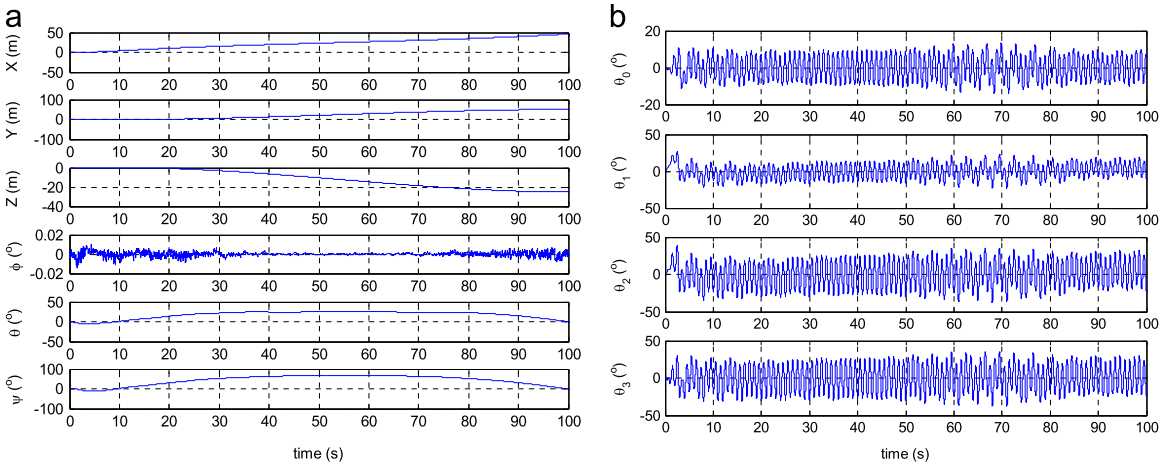

Fig. 19. Bezier curve tracking responses: (a) 6-DOF responses and (b) link angles.

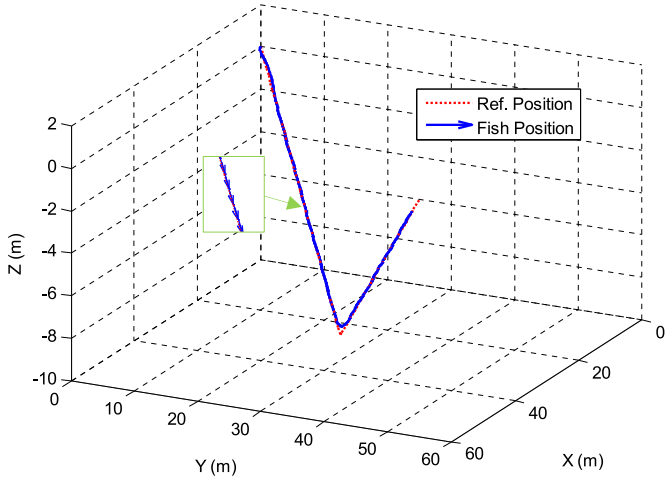

Fig. 20. Straight line tracking with descending and ascending swimming.

4.2. Speed control

A type 1 servo control (T1SC) with an LQR optimal state feedback technique was used to control the speed. Fig. 10(a) shows the regulated speed of linearized model while Fig. 10(b) shows the regulated speed of nonlinear model. The regulated speed from 0.2 m/s to 1 m/s indicates favorable performance of the fish robot without steady-state error in both cases. The simulations were conducted in ocean current perturbations at an ocean speed of 0.5 m/s ($|V_c|$=0.5 m/s).

4.3. Orientation tracking control

Type 1 servo control with the LQR optimal state feedback technique was used to control orientation. Fig. 11(a) and (b) show the orientation control, linear and nonlinear responses, with underwater stream perturbations.

Tracking response of the yaw angle between 0° and ±40° does not exhibit significant steady-state error and overshoot within the finite period from 7 s to 8 s approximately. Fig. 12(a) and (b) shows ±40° turning in 2-D motion.

4.4. Stabilization control

To ensure that the open-loop system was naturally stable, the buoyancy balancing tank was added. Step inputs were applied by moving m_x to 0.2 m, the center, and −0.2 m, and by moving m_y to 0.1 m, the center, and −0.1 m. The system was stable at pitch and roll angles of ±51.15° and ±32.06°, respectively. Fig. 13 shows the natural stability of the open-loop system.

A type 1 control system with LQR state feedback was adopted for 2-DOF stabilization. The input references were θ_{ref}= ±40° and

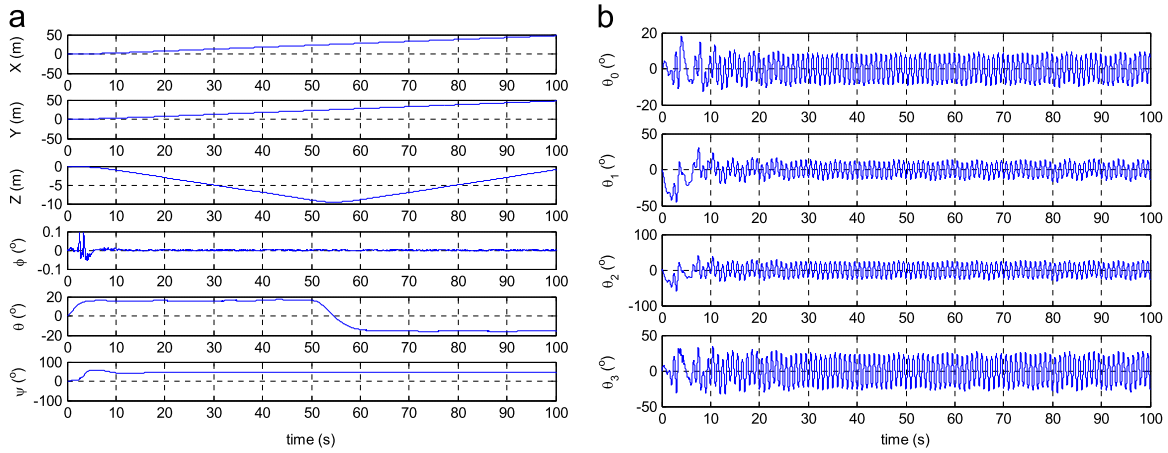

Fig. 21. Straight line tracking responses: (a) 6-DOF responses and (b) link angles.

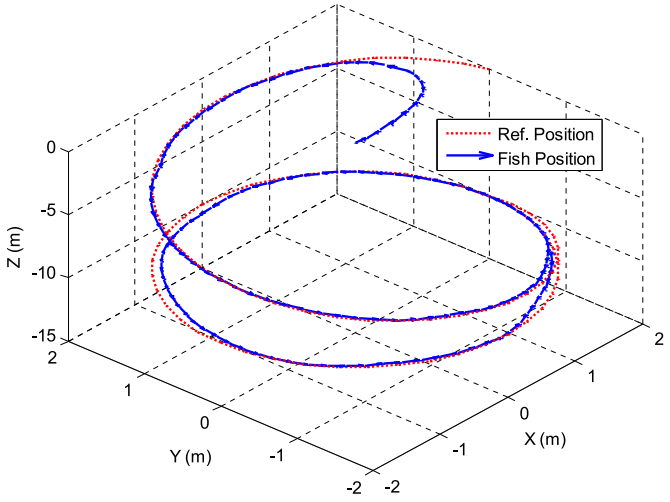

Fig. 22. The circular path reference tracking with a 2 m radius.

$\phi_{ref} = \pm 30°$. The closed-loop responses of the system show that the transient responses produced a settling time of 2.13 s and a final pitch angle value of $\pm 40°$. The roll angle produced a settling time of 2.6 s and a final value of $\pm 30°$. Key performance indices such as settling time and steady-state error etc. can be improved by adopting a controller, such as an LQR controller. Fig. 14(a) and (b) shows the simulation results of the controlled responses, which were achieved by applying the designed control law to the linear and nonlinear models of the stabilizing system. For the case of failure, the response after the fish stops moving is shown in Fig. 15.

4.5. 3-D trajectory tracking control

3-D swimming simulations were conducted in three types of trajectories with the measured global velocity (u) and yaw angle (ψ). Simulation results of the trajectory control responses were achieved by applying the proposed type 1 LQR controller to three nonlinear models of the fish robot, including all hydrodynamic forces, dynamics, and kinematics as mention in Section 2.

The fish robot first swam, tracked a Bezier curve, and swam downward. The controlled fish robot then swam, tracked a straight line, and successively descended and ascended. Finally, the fish robot swam, tracked a circular curve and performed descending and depth-regulated swimming successively. The tracking responses show the feasibility and the performance of the fish robot swimming in the NED reference frame within 100 s.

Fig. 16 shows the first tracking command (the Bezier curve) without ocean current perturbations. Alternatively, Fig. 17 shows that the swimming fish tracks the same reference in an ocean current environment ($|V_c| = 0.5$ m/s), with a small averaged error of approximately (0.34, 0.55, 0.24) m. The results of the comparison between surroundings with and without an ocean flow were not significantly different.

Fig. 18(a) shows the robot fish swimming by following the reference curve along the X and Y axes. The simulation started from the initial condition at 5 m on the Y axis. The controlled fish robot then attempted to swim back to track the reference curve and kept swimming along the reference curve, with a small tracking error, until it reached the final position $(x_{final}, y_{final}) = (50, 50)$ (m).

Fig. 18(b) shows the 2-D tracking response display along the X and Z axes. This simulation started with an initial depth of -5 m. The controlled fish robot swam back to the reference curve and tracked the surge and heave with a small tracking error until it reached the final position $(x_{final}, z_{final}) = (50, -25)$ (m).

The 6-DOF motion responses—which are surge, sway, heave, roll, pitch, and yaw – during Bezier curve tracking are shown in Fig. 19(a). Fig. 19(b) shows the tail link behavior. During tracking, the robot fish swings and folds its tail to regulate its position in 3-D space.

Fig. 20 shows the straight reference line of descending and ascending swimming for the second swimming scenario. The robot fish initially oriented itself at 45° and swam and tracked the straight line until it reached the final waypoint $(x_{final}, y_{final}, z_{final}) = (50, 50, 0)$ (m), with a small steady state error approximate to (0.35, 0.25, 0.09) m and a small averaged error (0.41, 0.40, 0.04) m.

During tracking, the barycenter mechanism controls descending and ascending swimming by adjusting the pitch angle. The result of heave controlling shows smooth descending and ascending swimming with arrows indicating direction in Fig. 20. Fig. 21(a) shows the 6-DOF motion responses for straight line tracking and Fig. 21(b) shows the tail link behaviors. During tracking, the robot fish swings its tail with less tail folding when regulating its position.

A circular path was set as a reference trajectory for the fish robot. The fish robot was made to swim around in CW and CCW directions and regulate its depth while simultaneously swimming and turning. The result of circular tracking in a CCW direction with a radius of 2 m is depicted in Fig. 22.

The swimming pattern started from the origin at (0, 0, 0) m. The robot fish then turned its head in a CCW direction to track the reference trajectory as the depth changed. In the descending

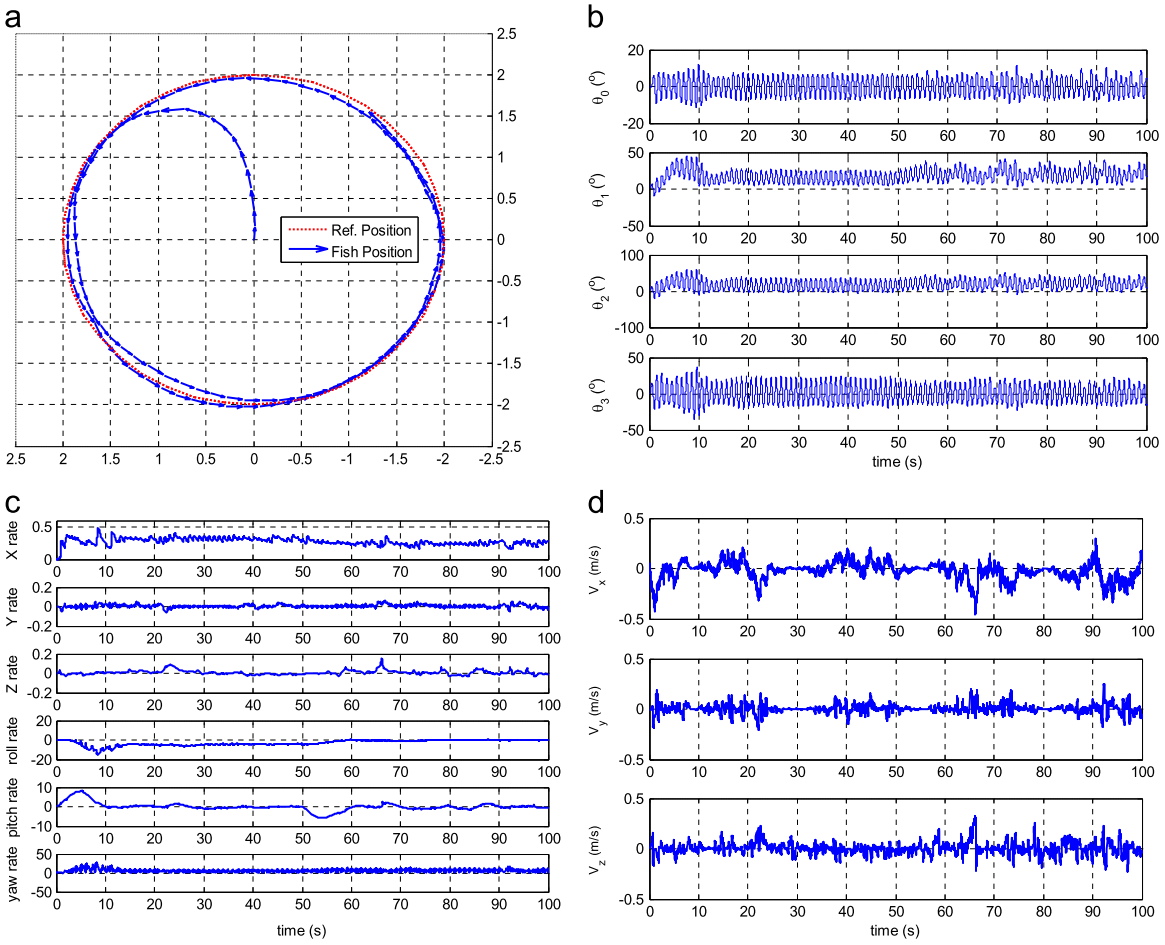

Fig. 23. Circular reference tracking: (a) trajectory tracking, (b) link angles for tracking, (c) velocity responses for tracking, and (d) current velocities acting on the fish robot body for tracking.

swimming mode, the steady-state errors were 0.32 m, 0.49 m, and 0.03 m for the surge, sway, and heave motions, respectively. The results show small errors with averaged error (0.07, 0.04, 0.51) m. In depth regulating mode, the robot fish tracked the trajectory and depth commands with a small tracking error (as with the previous results) and maintained smooth tracking behavior until it reached its target point at (2, 0, −10) m.

Fig. 23(a) shows circular tracking swimming in the *X*–*Y* plane. The headings are denoted by arrow marks. Fig. 23(b) shows the tail link behaviors. When circular tracking, the fish robot constantly folds and swings its tail while regulating its swimming position. Fish velocity responses for circular tracking are shown in Fig. 23(c). Fig. 23(d) illustrates the ocean current perturbations for circular tracking during swimming, respectively.

All of the simulation results – for the mathematical models with and without control – demonstrate the feasible operation and reasonable tracking performance of the fish robot in 3-D motion based on the representative reference trajectories. The feasibility of the proposed control design is reflected in the maneuverability and tracking performance in ocean flow surroundings.

Although a linear controller may not ensure system performance and stability at all equilibrium points, the proposed controllers that were used to control the three separate behaviors indicated that an easy control design scheme is applicable to the original nonlinear system. This is because a system with an LQR state feedback design ensures a certain amount of stability robustness (Anderson & Moore, 1989). However, a sophisticated robust control design is being implemented to ensure high performance and to guarantee the system abilities of fish robots subject to various uncertainties and underwater environments.

5. Conclusion and future work

This study develops and presents the details of a 6-DOF mathematical model for a robotic fish. The model considers the effects of fish swimming in ocean currents, similar to AUVs. The 2-DOF barycenter mechanism is proposed and demonstrated to stabilize the fish robot. Propulsive, turning, and stabilizing behaviors were merged and used to achieve fish robot motion and maneuverability in 3-D space. The simulation results validate satisfactory performances in maneuverability and path-tracking control for several reference trajectories (i.e., a Bezier curve, straight line, and circle). Descending swimming, ascending swimming, and depth regulation patterns were achieved by using the proposed barycenter mechanism to control the pitch angle of the fish robot body in the NED frame. Similarly, self-stabilization of the roll angle was achieved by controlling this mechanism. Future studies should improve the performance of the robot and adopt robust controls to prevent modeling uncertainty and underwater perturbations.

Acknowledgment

This research was sponsored by National Science Council Taiwan, ROC under the Grant NSC-102- 2218-E- 005-012.

Appendix. List of notations for linear control system

u	swimming velocity of fish robot
a_u, b_u, c_u	linearized parameters of fish velocity model
A_T	amplitude of input torque
u_r	referent input for fish velocity tracking system
ξ_u	tracking error of fish velocity tracking system
J_u	performance index of fish velocity tracking system
$\mathbf{e}_u$	state vector of fish velocity tracking system
u_u	input of fish velocity tracking system
Q_u, r_u	weighing matrix for fish velocity tracking system
$\widehat{A}_u$, $\widehat{B}_u$	system matrix of fish velocity tracking system
P_u	unique solution of Riccati equation for fish velocity tracking system
u_{ue}	control law of fish velocity tracking system
K_u	state feedback gain of fish velocity tracking system
K_u^I	error integral gain of fish velocity tracking system
$\mathbf{d}$	state vector of fish orientation model
ψ	yaw angle of fish orientation model
r	yaw angular velocity of fish orientation model
v	sway velocity of fish orientation model
A_r, B_r, C_r	linearized system matrix of fish orientation model
φ_T	total folding angle of the fish tail
b_r, b_v, c_r	turning, sway, and output gains of fish orientation tracking system
ψ_r	referent input for fish orientation tracking system
ξ_r	tracking error of fish orientation tracking system
$\widehat{y_r}$	output state of fish orientation tracking system
$\mathbf{s}$	state vector of fish stabilizing model
θ, $\dot{\theta}$	pitch angle and pitch velocity of fish stabilizing model
ϕ, $\dot{\phi}$	roll angle and roll velocity of fish stabilizing model
A_s, B_s, C_s	linearized system matrix of fish stabilizing model
$\mathbf{u_s}$	input vector of fish stabilizing model
$\boldsymbol{\xi_r}$	referent input vector of fish stabilizing tracking system
ϕ_r, θ_r	referent input for roll angle and pitch angle of fish stabilizing tracking system
ξ_ϕ, ξ_θ	tracking error for roll angle and pitch angle of fish stabilizing tracking system

References

Sfakiotakis, M., Lane, D. M., Bruce, J., & Davies, C. (1999). Review of fish swimming modes for aquatic locomotion. *IEEE Journal of Oceanic Engineering*, *24*(2), 237–252.

Colgate, J. E., & Lynch, K. M. (2004). Mechanics and control of swimming: a review. *IEEE Journal of Oceanic Engineering*, *29*(3), 660–673.

Hoar, W. S., & Randall, D. J. (1978). *Fish Physiology*. vol. VII. New York: Academic Press.

Anderson, J. M., & Chhabra, N. K. (2002). Maneuvering and stability performance of a robotic tuna. *Integrative and Comparative Biology*, *42*(1), 118–126.

Donley, J. M., & Dickson, K. A. (2000). Swimming kinematics of juvenile kawakawa tuna (*Euthynnus Affinis*) and chub mackerel (*Scomber Japonnicus*). *Journal of Experimental Biology*, *203*, 3103–3116.

Wen, L., Wang, T., Wu, G., & Liang, J. (2013). Quantitative thrust efficiency of a self-propulsive robotic fish: experimental method and hydrodynamic investigation. *IEEE/ASME Transaction on Mechatronics*, *18*(3), 1027–1038.

Nakashima, M., & Ohgishi, N. (2003). A study on the propulsive mechanism of a double jointed fish robot utilizing self-excitation control. *International Journal Japan Society of Mechanical Engineering*, *46*(3), 982–990.

Yu, J., & Wang, L. (2005). Parameter optimization of simplified propulsive model for biomimetic robot fish. In *Proceeding of IEEE International Conference on Robotics and Automation* (pp. 3306–3311). Barcelona, Spain.

Kim, H. S., Lee, B. R., Vo, T. Q., & Trung, Q. B. (2008). A study on optimization of fish robot velocity using genetic algorithm. In *Proceeding of IEEE International Conference on Smart Manufacturing Application* (pp. 441–446). Gyeonggi-do, Korea.

Vo, T. Q., Kim, H. S., Cho, H. S., Dang, D. N., & Lee, B. R., (2009). A study on optimization of fish robot maximum velocity using the combination of genetic-hill climbing algorithm. In *Proceeding of ICROS-SICE International Joint Conference* (pp. 2280–2285). Fukuoka, Japan.

Vo, T. Q., Kim, H. S., & Lee, B. R. (2012). Smooth gait optimization of a fish robot using the genetic-hill climbing algorithm. *Journal of Robotica*, *30*(2), 257–278.

Niku, S. B. (2001). *Introduction to Robotics Analysis, System, Application*. Practice Hall, Upper Saddle River, New Jersey.

Lighthill, M. J. (1960). Note on the swimming of slender fish. *Journal of Fluid Mechanics*, *9*, 305–317.

Suebsaiprom, P., & Lin, C. L. (2012). Fish-tail modeling for fish robot. In *Proceeding of IEEE International Symposium on Computer, Consumer and Control* (pp. 548–551). Taichung, Taiwan.

Suebsaiprom, P., Lin, C. L., & Saimek, S. (2012). Fish robot modeling and simulation: Fish-tail and rigid-body motion. *International Journal of Advancements in Computing Technology*, *4*(8), 105–114.

Yu, J. Z., Liu, L. H., & Wang, L. (2006). Dynamic and control of turning maneuver for biomimetic robotic fish. In *Proceeding of IEEE International Conference on Intelligent Robots and Systems* (pp. 5400–5405). Beijing, China.

Yu, J. Z., Tan, M., Wang, S., & Chen, E. (2004). Development of a biomimetic robotic fish and its control algorithm. *IEEE Transaction on Systems, Man, and Cybernetics*, *34*(4), 1798–1810.

Suebsaiprom, P., Saimek, S., & Chaisawadi, A. (2004). Water level control for stabilizing platform. In *Proceeding of International Conference on ECTI* (pp. 226–229). Cholburi, Thailand.

Liu, L. Z., Yu, J. Z., & Wang, L. (2006). Dynamic modeling of three-dimensional swimming for biomimetic robotic fish. In *Proceeding of IEEE International Conference on Intelligent Robots and Systems* (pp. 3916–3921). Beijing, China.

Morgansen, K. A., Triplett, B. I., & Klein, D. J. (2007). Geometric methods for modeling and control of free-swimming fin-actuated underwater vehicles. *IEEE Transaction on Robotics*, *23*(6), 1184–1198.

Zhou, C., Cao, Z. Q., Wang, S., & Tan, M. (2006). The posture control and 3-D locomotion implementation of biomimetic robot fish. In *Proceeding of IEEE International Conference on Intelligent Robots and Systems* (pp. 5406–5411). Beijing, China.

Refsnes, J. E., Sorensen, A. J., & Pettersen, K. Y. (2008). Model-based output feedback control of slender-body underactuated AUVs: Theory and experiments. *IEEE Transaction on Control Systems Technology*, *16*(5), 930–946.

Refsnes, J. E. (2007). *Nonlinear model-based control of slender body AUVs*. Norway: Norwegian University of Science and Technology.

Suebsaiprom, P., & Lin, C. L. (2013). 2-DOF barycenter mechanism for stabilization of fish-robots. In *Proceeding of IEEE International Conference on Industrial Electronics and Applications* (pp. 1119–1122). Melbourne, Australia.

Silvestre, C., Cunha, R., Paulino, N., & Pascoal, A. (2009). A bottom-following preview controller for autonomous underwater vehicles. *IEEE Transaction on Control Systems Technology*, *17*(2), 257–266.

Healey, A. J., & Lienard, D. (1993). Multivariable sliding-mode control for autonomous diving and steering of unmanned underwater vehicles. *IEEE Journal of Oceanic Engineering*, *18*(3), 327–339.

Busch, R. (2009). *Modelling and simulation of an autonomous underwater vehicle* (M. S. thesis). South Africa: University of Stellenbosch.

Bo, W., Lei, W., Ru, X. Y., & Bai, Q. Z. (2009). Model and simulation of a mini AUV in spatial motion. *Journal of Marine Science Application*, *8*(1), 7–12.

Cook, M. V. (2007). *Flight dynamics principles: A linear systems approach to aircraft stability and control*. Burlington: Elsevier Aerospace Engineering Series.

Pietsch, T. W. (2014). *Biology of fished: Locomotion mechanism; modes swimming; anguilliform versus carangiform swimming*. Washington: University of Washington Lecture Note.

Borazjani, I. (2008). *Numerical simulations of fluid–structure interaction problems in biological flows*. USA: University of Minnesota.

Lauder, G. V., & Madden, P. G. A. (2006). Learning from fish: Kinematics and experimental hydrodynamics for roboticists. *International Journal of Automation and Computing*, *3*(4), 325–335.

Cooney, L. A. (2006). *Dynamic response and maneuvering strategies of a hybrid autonomous underwater vehicle in hovering* M.S. thesis. USA: Massachusetts Institute of Technology.

Ogata, K. (1994). *Designing linear control systems with MATLAB*. New Jersey: Prentice Hall.

McGookin, E. W., Murray-Smith, D. J., Li, Y., & Fossen, T. I. (2000). Ship steering control system optimization using genetic algorithms. *Control Engineering Practice*, *8*(4), 429–443.

Chan, W. L., & Kang, T. (2011). Simultaneous determination of drag coefficient and added mass. *IEEE Journal of Oceanic Engineering*, *36*(3), 422–430.

Techet, A. H. (2005). *Marine hydrodynamics*. Massachusetts Institute of Technology Lecture Note 14: Version 3. Massachusetts, USA.

Perrault, D., Bose, N., Young, S. O., & Williams, C. D. (2003). Sensitivity of AUV response to variations in hydrodynamic parameters. *Ocean Engineering*, *30*(6), 779–811.

Saout, O., & Ananthakrishnan, P. (2011). Hydrodynamic and dynamic analysis to determine the directional stability of an underwater vehicle near a free surface. *Applied Ocean Research*, *33*(2), 158–167.

Anderson, B. D. O., & Moore, J. B. (1989). *Optimal control: linear quadratic methods*. Prentice-Hall, Englewood Cliffs.